Understanding Hematopoietic Stem Cell Development through Functional Correlation of Their Proliferative Status with the Intra-aortic Cluster Architecture

Stem Cell Reports

Understanding haematopoietic stem cell development through functional correlation of their proliferative status with the intra-aortic cluster architecture

--Manuscript Draft--

Manuscript Number:	STEM-CELL-REPORTS-D-16-00648R1
Article Type:	Research Article
Keywords:	Haematopoietic stem cells; Fucci; proliferation
Corresponding Author:	Alexander Medvinsky MRC Centre for Regenerative Medicine Edinburgh, UNITED KINGDOM
First Author:	Antoniana Batsivari, PhD
Order of Authors:	Antoniana Batsivari, PhD
	Stanislav Rybtsov, PhD
	Céline Souilhol, PhD
	Anahi Binagui-Casas
	David Hills, PhD
	Suling Zhao
	Paul Travers, PhD
	Alexander Medvinsky, PhD
Abstract:	During development, haematopoietic stem cells (HSC) emerge in the aorta-gonad-mesonephros (AGM) region through a process of multistep maturation and expansion. While proliferation of adult HSCs is implicated in the balance between self-renewal and differentiation, very little is known about the proliferation status of nascent HSCs in the AGM region. Using Fucci reporter mice that enable in vivo visualisation of cell cycle status, we detect increased proliferation during pre-HSC expansion followed by a slowing down of cycling once cells start to acquire a definitive HSC state, similar to foetal liver HSCs. We observe time-specific changes in intra-aortic clusters corresponding to HSC maturation stages. The proliferative architecture of the clusters is maintained in an orderly anatomical manner with slowly cycling cells at the base and more actively proliferating cells at the more apical part of the cluster, which correlates with c-Kit expression levels, thus providing an anatomical basis for the role of SCF in HSC maturation.

Understanding haematopoietic stem cell development through functional correlation of their proliferative status with the intra-aortic cluster architecture

A. Batsivari[1], S. Rybtsov[1], C. Souilhol[2], A. Binagui-Casas[1], D. Hills[1], S. Zhao[1], P. Travers[1], A. Medvinsky[1]

[1]Institute for Stem Cell Research, Medical Research Council Centre for Regenerative Medicine, University of Edinburgh, SCRM Bioquarter, 5 Little France Drive, Edinburgh EH16 4UU, Scotland, UK.

[2]Department of Infection, Immunity & Cardiovascular Disease, University of Sheffield, UK.

*Corresponding author: Alexander Medvinsky, email: A.Medvinsky@ed.ac.uk; tel. (+44) (0)131 651 9556.

Abstract

During development, haematopoietic stem cells (HSC) emerge in the aorta-gonad-mesonephros (AGM) region through a process of multistep maturation and expansion. While proliferation of adult HSCs is implicated in the balance between self-renewal and differentiation, very little is known about the proliferation status of nascent HSCs in the AGM region. Using Fucci reporter mice that enable *in vivo* visualisation of cell cycle status, we detect increased proliferation during pre-HSC expansion followed by a slowing down of cycling once cells start to acquire a definitive HSC state, similar to foetal liver HSCs. We observe time-specific changes in intra-aortic clusters corresponding to HSC maturation stages. The proliferative architecture of the clusters is maintained in an orderly anatomical manner with slowly cycling cells at the base and more actively proliferating cells at the more apical part of the cluster, which correlates with c-Kit expression levels, thus providing an anatomical basis for the role of SCF in HSC maturation.

Introduction

The AGM region plays an important role in development of HSCs that give rise to the adult haematopoietic system (Kumaravelu et al. 2002; Medvinsky & Dzierzak 1996; Müller et al. 1994; Medvinsky et al. 2011; Ciau-Uitz et al. 2016). The pool of immature precursors (pre-HSCs), which cannot yet repopulate adult irradiated recipients, gradually expands and matures in the AGM region (Rybtsov et al., 2016). This concealed dramatic expansion of pre-HSCs culminates in emergence of a few definitive (d)HSCs in the E11 AGM region followed by a sudden increase in their number in the E12 foetal liver, detectable by direct transplantation into adult irradiated recipients (Kumaravelu et al. 2002; Ema & Nakauchi 2000; Rybtsov et al. 2016).

Cell proliferation is one of critical factors involved in many developmental processes (Budirahardja & Gönczy 2009; Lange & Calegari 2010; Kaldis & Richardson 2012) and the proliferative status of adult HSCs is an important feature of their biology. In the foetal liver, HSCs expand, probably through symmetric division until week 3-4 postnatally, and then become quiescent (Bowie et al. 2006). Proliferative quiescence in the adult maintains "stemness" of HSCs and prevents their exhaustion (Passegué et al. 2005; Wilson et al. 2008; Seita, Jun; Weissman 2010; Takizawa et al. 2011; Pietras et al. 2011; Nakamura-Ishizu et al. 2014). Physiological demands drive HSCs to enter proliferation, while a balance is maintained to ensure HSC self-renewal and differentiation. The bone marrow niche maintains HSC quiescence through essential signalling (Jude et al. 2008; Mendelson & Frenette 2014; Morrison & Scadden 2014). By contrast, downstream committed progenitors, which are involved in the immediate production of mature blood cells, are significantly more proliferative (Passegué et al. 2005).

Given the importance of proliferation in cell commitment and differentiation, we have studied here proliferative changes during HSC maturation steps, which to date has not been studied in detail. We showed previously that in culture developing HSCs of the AGM region proliferate slower than committed progenitors (Taoudi et al. 2008). More recent *in vivo* analysis of the dramatic pre-HSC expansion in the AGM region suggests that either proliferation or/and cell recruitment may play a role (Rybtsov et al. 2016).

In vitro modelling has proved to be a powerful and informative approach to the identification of pre-HSC states and dissection of HSC developmental mechanisms (Taoudi et al. 2008). HSCs develop through a multi-step process: proHSC → preHSC I → preHSC II → dHSC, which involves sequential upregulation of haematopoietic markers CD41 (Itga2b), Runx1 (AML1), CD43 (Spn) and CD45 (Ptprc) in VE-cadherin^{+} (VC) precursors (Rybtsov et al. 2014; Rybtsov et al. 2011; Taoudi et al. 2008; Medvinsky & Dzierzak 1996; Liakhovitskaia et al. 2014; Swiers et al. 2013; Yoder et al. 1997). Pro-HSCs (VC^{+}CD41^{lo}CD43^{-}CD45^{-}) emerge at E9.5, pre-HSCs Type I (VC^{+}CD41^{lo}CD43^{+}CD45^{-}) at E10.5 and pre-HSCs Type II (VC^{+}CD41^{lo}CD43^{+}CD45^{+}) appear at E11.5 stages. Low dHSCs numbers emerge at E11.5 and, although phenotypically similar to pre-HSCs Type II, they can be detected by direct transplantations into irradiated recipients. Pro/pre-HSCs have been identified in intra-aortic haematopoietic clusters budding from the endothelium of major embryonic arteries (Rybtsov et al. 2011; Rybtsov et al. 2014; Taoudi et al. 2008; Yokomizo & Dzierzak 2010; Kissa & Herbomel 2010; Boisset et al. 2011; Gordon-Keylock et al. 2013; Ciau-Uitz et al. 2016).

Functional assessment of cell proliferation in live cells often involves Hoechst staining, which can be toxic and alter the experimental outcome (Parish 1999). Instead, we used the fluorescent ubiquitination-based reporter (Fucci) system, which enables non-invasive *in vivo* visualisation of the cell cycle status and their isolation for functional analysis (Sakaue-Sawano et al. 2008; Yo et al. 2015; Zielke & Edgar 2015).

We describe here that pro-HSCs (at E9.5), initially slowly cycle, then enter active proliferation during E10.5 - E11.5, which correlates with the expansion of the pro/pre-HSC pool (Rybtsov et al. 2016). However, this phase is followed by gradual slowing down of proliferation, the first signs of which can be observed already in AGM dHSCs, in keeping with gradual acquisition of adult status by dHSCs. We also describe the orderly architectural evolvement of intra-aortic clusters in which step-wise HSC maturation and proliferation are linked. It is suggested that the proliferative pattern within the cluster is defined by SCF/cKit signalling.

Results

Changes in proliferative status of developing HSCs

To analyse the proliferative status of developing HSCs, we used the Fucci dual reporter mouse lines (see Experimental Procedures) appropriate for analysis of the haematopoietic system (Yo et al. 2015a; Zielke & Edgar 2015). Two antiphase oscillating proteins that mark cell cycle transitions Cdt1 (genetically labelled by the red fluorescent protein mKO2) and Geminin (genetically labelled by the green fluorescent protein, mAG), which are controlled by the cell cycle machinery through proteasomal degradation, have been used here as reporters. Cdt1-mKO2 is expressed during G_0 and G_1 phases and the cells fluoresce red, while Geminin-mAG (Gem-mAG) marks green the cells that are in $S/G_2/M$ phases (Fig. 1A). During the G_1/S transition cells become yellow and no reporter is expressed in early G_1 phase (shown as grey) (Fig. 1A). Therefore, slowly cycling populations are represented mainly by red (Cdt1-mKO2$^+$) cells and actively cycling populations are mainly green (Gem-mAG$^+$) cells.

Flow cytometry analysis of Fucci reporter embryos showed that in the caudal part of the E9.5 embryo endothelial cells were mainly within $S/G_2/M$ and early G_1 phases, indicating that they were actively proliferative. Only 6.6% (±1.6) of the endothelial population (VC$^+$CD45$^-$CD41$^-$CD43$^-$) were found in the G_0/G_1 phases of the cell cycle (vs 54.8% ±11.9 in $S/G_2/M$, p=0.0002) (Fig. S1A, S1B). By contrast, a significant proportion of cells in the pro-HSC population (VC$^+$CD45$^-$CD41^{lo}CD43$^-$) were in G_0/G_1 phases (23.7% ±7.6 vs G_0/G_1 endothelial population, p=0.004), suggesting that a fraction of these cells emerging from the endothelium slow down their cycling (Fig. 1C). Compared to the pro-HSC population, more committed haematopoietic progenitors (VC$^-$CD45$^-$CD41^{lo}CD43$^+$) (Rybtsov et al. 2014) were actively proliferating (progenitors: 8.6%±9.3 vs pro-HSC: 23.7%±7.6 in G_0/G_1, p=0.02) (Fig. 1C). To functionally define the cell cycle status of pro-HSCs, Gem-mAG$^+$ and Gem-mAG$^-$ fractions of this population were sorted from Fucci embryos, co-aggregated with OP9 cells for 7 days in culture and then transplanted into irradiated recipients, as described previously (Rybtsov et al. 2014)(Fig. 1B). Only the Gem-mAG$^-$ fraction generated transplantable dHSCs suggesting that pro-HSCs are slowly cycling (Fig. 1D & Table S1). Meanwhile, both, Gem-mAG$^+$ and Gem-mAG$^-$ fractions of the pro-HSC population were able to generate colonies of myeloid cells in CFU-C assays (Fig. S1C).

While the E9.5 endothelium is mainly proliferating, this population slows down their cycle during the following days of development since the proportion of G_0/G_1 endothelial cells increased to 47% (±6.1) by E11.5 (vs E9.5: 6.6% ±1.6, p<0.0001) (Fig. S1B). In contrast to pro-HSCs observed in E9.5-10.5 embryos, the proportion of E10.5 pre-HSC Type I ($VC^+CD45^-CD41^{lo}CD43^+$) in the G_0/G_1 phases decreased to 8.5% (±6.7) (vs E10.5 pro-HSC: 19.2%±4, p=0.03), suggesting that by this stage the HSC lineage becomes more proliferative (Fig. 1C). Indeed, functional validation using *ex vivo* maturation and transplantation showed that in contrast to E9.5 pro-HSCs, pre-HSC Type I resided in both the Gem-mAG^+ and Gem-mAG^- fraction, which is in line with the dramatic expansion of the pre-HSC pool at E10.5 (Fig. 1D & Table S1) (Rybtsov et al. 2016). We observed higher repopulation levels from the Gem-mAG^+ fraction but no bias in multi-lineage differentiation compared to the Gem-mAG^- fraction (data not shown). Similar to the E9.5 pro-HSC population, both Gem-mAG^+ and Gem-mAG^- fractions of E10.5 pre-HSC Type I were equally capable of generating myeloid colonies in the methylcellulose (Fig. S1C).

By E11.5 immunophenotypic analysis showed a dramatic increase of G_0/G_1 cells in the pre-HSC Type I population compared to E10.5, from 8.5% ±6.7 to 51.3% ±10.3 (p=0.02), respectively (Fig. 1C). By contrast, the more advanced pre-HSC Type II population ($VC^+CD45^+CD41^{lo}CD43^+Sca1^+$) was found mainly in early G_1 and $S/G_2/M$ phases associated with active cell cycling (19.3±12.8 and 50.7±3.7, respectively vs G_0/G_1: 19.7±7.9, p=0.02) (Fig. 1C). Previous analysis showed that pre-HSCs emerge predominantly in the ventral domain of the dorsal aorta (AoV) with some contribution from the dorsal domain (AoD) (Souilhol et al. 2016; Taoudi & Medvinsky 2007). Interestingly, immunophenotypic analysis at E11.5 revealed a larger proportion of the pre-HSC Type I population in $S/G_2/M$ phases from the AoD compared to AoV (30% ±7.1 vs 16.1% ±8.7 respectively, p=0.02), which is reminiscent of committed progenitor cells (Fig. S1B). By contrast, no proliferative difference was observed between AoV- and AoD-derived endothelial or pre-HSC Type II populations (data not shown).

A striking change in cell cycle status was observed in pre-HSC Type I by E11.5. Functional transplantations demonstrated that in contrast to E10.5, these cells resided almost exclusively in G_0/G_1, with only a few low repopulating cells residing in $S/G_2/M$ phases (Fig. 1D, S1D, Table S1). By contrast,

pre-HSCs Type II were found in both Gem-mAG$^+$ and Gem-mAG$^-$ fractions (Fig. 1D). Notably, direct transplantations (without prior culturing) showed that mature E11.5 dHSCs were in G_0/G_1 phases, indicating that acquisition of the adult status is accompanied by reducing cycling (Fig. 1D & Table S1). Although both E11.5 pre-HSCs and dHSCs were predominantly Gem-mAG$^-$, CFU-Cs were equally well represented by both Gem-mAG$^+$ and Gem-mAG$^-$ fractions (Fig. S1C).

When we analysed E14.5 foetal liver we found that the majority of HSCs were also within G_0/G_1 or early G_1 phases (G_0/G_1: 44.8%±6.7) and became quiescent in the adult bone marrow (G_0/G_1: 93.1%±1.4) (Fig. S1B), in contrast to restricted progenitors (G_0/G_1: 10.2%±0.8 in FL, p=0.0005 and G_0/G_1: 69.2.8%±2.6 in BM, p=0.0002) (Fig. S1B). These findings in combination with transplantation assays (Fig. 1E & Table S1) are in line with previous reports (Bowie et al. 2006; Bowie et al. 2007; Passegué et al. 2005). Based on limiting dilution transplantation analysis, the numbers of foetal liver HSCs in G_0/G_1 phase were 17/100 cells and in $S/G_2/M$ phases were 0.3/100 cells.

Proliferative structure of intra-aortic haematopoietic clusters

HSCs and more committed progenitors develop in intra-arterial haematopoietic clusters at E10.5 that are budding from the endothelium of major arteries by E10.5 (Garcia-Porrero et al. 1995; North et al. 1999; Yokomizo & Dzierzak 2010; Rybtsov et al. 2011; Boisset et al. 2015). Fucci mice allowed us to visualise the cell cycle status of cells within intra-aortic clusters. In the E9.5 embryo caudal part, haematopoiesis occurs in two locations: pro-HSCs (CD41$^+$CD43$^-$) develop in the dorsal aorta and committed progenitors (CD41$^+$CD43$^+$) form a string of large clusters in the omphalomesenteric artery (OMA) (Zovein et al. 2010; Rybtsov et al. 2014). Haematopoietic cells are marked in these locations by the transcription factor Runx1, including flat cells integrated in the endothelial lining of the dorsal aorta (Fig. 2A, A′) (Swiers et al. 2013; Rybtsov et al. 2014). We sought to identify candidate pro-HSCs using the Fucci reporters. We found a few VC$^+$Runx1$^+$ cells, closely associated with the endothelium of the dorsal aorta, which are labelled by CD41 but not CD43 (Fig. 2A, A′, S2A, S2A′) and which were also Cdt1-mKO2$^+$ (Geminin-mAG$^-$) (Fig. 2B, B′), characteristic of pro-HSCs identified by functional analysis (Fig. 1D). It is conceivable that low expressing CD41 cells were not detectable using this

immunofluorescence analysis. Our previous study showed that committed progenitors localised in the OMA are labelled by CD43 (Rybtsov et al. 2014). Indicative of their active proliferation, the majority of OMA $CD43^+$ cells were Geminin-mAG^+ (Cdt1-$mKO2^-$) both by flow cytometry (Fig. 1C) and confocal analysis (Fig. 2C, C′, S2B, S2B′).

It is reasonable to think that intra-aortic cell clusters are formed through budding from the endothelium of the dorsal aorta and may gradually build up through proliferation. Confocal analysis showed that the base of E10.5 clusters was $VC^+CD41^+Runx1^+$ (and also c-Kit^+) but not $CD43^+$ and therefore harboured the most immature pro-HSC population (Fig. 3B, B′, S3). Notably, these cells closely associated with endothelium were in G_0/G_1 phases (Geminin-mAG^-/Cdt1-$mKO2^+$) (Fig. 3A) as E9.5 pro-HSCs (Fig. 1D). These G_0/G_1 cells at the base were observed in 67-100% of clusters in four analysed embryos (Table 1A). Meanwhile, more apically located cells, presumably derived from the basal cells, were in $S/G_2/M$ phases (Geminin-mAG^+/Cdt1-$mKO2^-$). Among these actively proliferating more apical cells were the $VC^+CD43^+CD45^-$ pre-HSC Type I population and the committed $VC^+CD43^+CD45^+$ progenitor population (note pre-HSC Type II are rare at this stage (Fig. 3B, B′, S2C, S2C′) (Rybtsov et al. 2011; Rybtsov et al. 2014). Similar polarized basal-apical organization was observed in the usually significantly larger haematopoietic clusters of extra-embryonic (vitelline and umbilical) arteries (Fig. S4A).

By the next day (E11.5), when HSC precursors mature further, we analysed phenotypic changes in intra-aortic clusters. The base of E11.5 intra-aortic clusters was again represented by cells mainly in G_0/G_1 phases (Geminin-mAG^-/Cdt1-$mKO2^+$), which by this time upregulated CD43 and acquired a pre-HSC Type I phenotype (Fig. 3C, C′), as observed in 40-80% of clusters in individual embryos (n=5) (Table 1B). More apically located cells upregulated $CD45^+$ and thus acquired pre-HSC Type II phenotype and as expected from functional transplantation studies are both Geminin-mAG^+ and Geminin-mAG^- (Fig. 3C, C′).

Although Fucci analysis allowed us to visualize key phases of the cell cycle in the developing HSC lineage, this does not explain whether the cells are resting or cycling. To address this issue, we used antibody staining for Ki67 and found that all cells in the cluster including those which are at its base

(Cdt1^{+}), were cycling (Fig. 3D). Thus, Fucci analysis here reveals differences not between quiescent and cycling, but between slowly and rapidly cycling cells within the developing HSC lineage in the AGM region.

c-Kit expression correlates with cell cycle status in HSC precursors

The c-Kit/SCF signalling pathway is critically important for HSC development in the AGM region and in adult HSC niches (Rybtsov et al. 2014; Ding et al. 2012). Asymmetric, ventrally polarized expression of SCF in the AGM region correlates with predominant formation of intra-aortic clusters in the floor of the dorsal aorta (Souilhol et al. 2016). Our analysis of E10.5 clusters showed that c-Kit low cells in both intra-aortic and umbilical arteries were in G_0/G_1 phases, suggesting that they are slowly cycling (Fig. 4A, A′, S4C, S4C′ - white arrows). Although we observed c-Kit^{low} slowly proliferating cells in various positions, these were mostly localized to the base of the cluster, closely associated with endothelium (Fig. 4A, A′). By contrast, high c-Kit levels correlated with actively proliferating Geminin-mAG^{+} cells localised mainly apically in the cluster (Fig. 4A, A′, S4C, S4C′ - white arrowheads). Accordingly, slowly cycling pre-HSCs Type I (as shown functionally, Fig. E11.5-1D) were enriched for c-Kit low cells (G_0/G_1: 53.2%±7.4 are c-Kit^{lo} vs 5.3%±1.7 are c-Kit^{hi}, p=0.0006) compared to more actively cycling pre-HSC Type II (G_0/G_1: 48.1%±3.3 are c-Kit^{lo} vs 51.3%±3.2 are c-Kit^{hi}, p=ns and S/G_2/M: 19.9%±2.6 are c-Kit^{lo} vs 65.9%±4.9 are c-Kit^{hi}, p<0.0001)(Fig. 4B & Table S2), indicating that one of the roles of c-Kit/SCF signalling might be in expansion of the developing HSC pool (Rybtsov et al. 2016) through regulation of their proliferation (Bowie et al. 2007; Sasaki et al. 2010; Shin et al. 2014).

Discussion

Cell proliferation plays an important role in various developmental processes. It underlies growth of tissues and organs and is involved in cell fate decisions (Fuchs 2009; Pauklin & Vallier 2013). Proliferation is an important mechanism enabling self-renewal and differentiation of HSCs in the adult (Bowie et al. 2006; Pietras et al. 2011). Here we used Fucci reporter mice to define the proliferative status of the developing HSCs. Our conclusions based on the ratio of Geminin-mAG^{+} and Cdt1-mKO2^{+}

cells are consistent with previously described proliferation rates of foetal liver and bone marrow HSCs (Bowie et al. 2006; Nygren et al. 2006; Bowie et al. 2007; Takizawa et al. 2011; Fuchs 2009).

During maturation, the developing HSC pool undergoes massive expansion within the AGM region before colonization of the foetal liver (Rybtsov et al. 2016). HSC maturation occurs through sequential upregulation of haematopoietic markers (CD41, CD43, CD45) (Taoudi et al. 2008; Rybtsov et al. 2014). Fucci mice enabled visualisation and isolation of cells in G_0/G_1 (red) and $S/G_2/M$ (green) phases, so that developing HSCs could be studied at both the phenotypic and functional levels (Fig. 5A). We found that the Geminin-mAG$^-$ but not Geminin-mAG$^+$ fraction of the E9.5 pro-HSC population was able to mature into dHSCs, which could reconstitute adult irradiated recipients, indicating that pro-HSCs are non- or slowly cycling. By the next day (E10.5), upregulation of CD43 marks the emergence of pre-HSCs Type I, which are actively proliferating since both Geminin-mAG$^+$ and Geminin-mAG$^-$ fractions can produce dHSCs. Thus, proliferation likely underlies the previously described dramatic expansion of the pre-HSC pool (from 5 cells at early E10 to 50 cells by late E10.5) (Rybtsov et al. 2016). At E11.5 pre-HSCs Type II mature and continue to proliferate, with some bias towards the Geminin-mAG$^-$ fraction, indicating a slowing down in this process, which becomes apparent in dHSCs. This slowing down of the cell cycle continues further in foetal liver HSCs; and finally, in mainly quiescent bone marrow HSCs (Fig. 5A)(Bowie et al. 2007; Yo et al. 2015).

This study confirms our previous observations that certain states in HSC development can persist for longer than one developmental day (Rybtsov et al. 2016). However, while the proliferative status of E9.5 and E10.5 pro-HSCs is similar, pre-HSCs Type I at E11.5 differ from E10.5 by their slow cycling. The origin of the slowly cycling E11.5 pre-HSC Type I population is not clear. One possible scenario (Fig. 5A-scenario A) is that a fraction of proliferative E10.5 pre-HSCs Type I slows down their cycling and persists as Type I until E11.5. Another scenario (Fig. 5A-scenario B) is that a fraction of retarded E9.5 pro-HSCs matured into pre-HSC Type I while maintaining their slow cycling. Whether these distinct pre-HSC fractions can contribute to the heterogeneity of the adult HSC pool (Sieburg et al. 2010; Dykstra et al. 2007; Benz et al. 2012; Ema et al. 2014) needs further investigation. The G_0/G_1 status of E11.5 pre-HSC Type I observed here contradicts a recent study reporting that these cells are

predominantly in $S/G_2/M$ phases, which could be explained by their short-term monitoring of recipients that revealed committed progenitors rather than HSCs (Zhou et al. 2016).

The emergence of HSCs in the AGM region is manifested morphologically by the formation of intra-aortic haematopoietic clusters (Rybtsov et al. 2011; Rybtsov et al. 2014; Taoudi et al. 2008; Yokomizo & Dzierzak 2010; Kissa & Herbomel 2010; Boisset et al. 2011). Although this process has not been investigated in detail experimentally, it could be assumed that endothelial-derived HSC precursors proliferate and mature to form the cluster. Our current functional analysis using Fucci mice allowed us to better define the identity of developing HSCs and dynamically map their location within intra-aortic clusters in a stage-specific manner. The day before clusters are formed, at E9.5, single slowly cycling cells of the $VC^{+}Runx1^{+}CD41^{+}$ phenotype were found attached to the aortic endothelium. However, since levels of CD41 expression detected under the microscope and by flow cytometry cannot be directly correlated, given the presence of few pro-HSCs per embryo (Rybtsov et al. 2016), this raises the possibility that true, $CD41^{low}$ pro-HSCs escaped our analysis. By the next day when active formation of intra-aortic clusters occurs, slowly cycling (G_0/G_1) pro-HSCs remain associated with the endothelium at the base of the cluster, whereas actively cycling ($S/G_2/M$) pre-HSCs Type I emerge more apically (Fig. 5B). By E11.5, the base of clusters still consists of slowly cycling cells, but now these are more mature pre-HSC Type I. Again, more actively cycling pre-HSC Type II develop in more apical positions. This organization was observed in at least 50% of intra-aortic clusters in E10.5 and E11.5 embryos. Similarly structured, although often significantly larger, clusters were also observed in extra-embryonic arteries. This suggests that clusters are initiated by slowly cycling precursors, which give rise to more mature actively proliferating precursors moving towards apical positions. This organisation of clusters is maintained throughout their maturation, suggesting their growth through predominant expansion of more mature pre-HSCs. This maturation of clusters correlates with progressive quantitative expansion of the pre-HSC population identified functionally by transplantations (Rybtsov et al. 2016).

c-Kit/SCF signalling is essential for HSC biology (Ikuta & Weissman 1992; Thorén et al. 2008; Ding et al. 2012; Marcelo et al. 2013). We have shown that SCF is ventrally polarized in the AGM region

and is a key regulator of step-wise pro/pre-HSC transitions (Souilhol et al. 2015). c-Kit is expressed in pro/pre- and dHSCs and is a principal marker for HSCs in the adult animal (Rybtsov et al. 2014; Kiel et al. 2005). Since c-Kit/SCF signalling is implicated in regulation of proliferation (Sasaki et al. 2010; Ema et al. 2000; Bashamboo et al. 2006), we studied the organisation of c-Kit expressing cells in developing intra-aortic clusters and found that slowly cycling cells including those at the base of the cluster express low levels of c-Kit, whereas actively cycling cells express high levels of c-Kit. Although further experimentation is needed to understand this observation mechanistically, it suggests that the stratified proliferative architecture of the cluster is at least partly defined by c-Kit/SCF signalling. Our analysis provides a basis for investigation of cellular and molecular events in maturing intra-aortic clusters in connection with functional expansion of the pro/pre-HSC pool in the AGM region.

Cell proliferation plays an important role in various differentiation processes and needs to be tightly regulated, for example: lengthening G_1 phase increases differentiation of neural stem cells into neurons (Lange & Calegari 2010; Lange et al. 2009); cyclin D in human ES cells controls balance between neuroectoderm and endoderm specification (Pauklin & Vallier 2013); deletion of p27 cell cycle inhibitor prevents specification of haematopoietic cells from the yolk sac endothelium (Marcelo et al. 2013). The temporal kinetics of pre-HSC proliferation is well controlled: although mature foetal liver HSCs expand, their proliferative activity is decreasing compared to the AGM region and subsequently, in the adult bone marrow, switches into quiescence associated with low c-Kit expression, which is necessary to prevent exhaustion of the HSC pool (Thorén et al. 2008; Matsuoka et al. 2011; Shin et al. 2014). Although our data indicate that pre-HSC expansion within the AGM region is driven by proliferation, it needs to be elucidated in future whether stage-specific proliferative changes *per se* play a role in HSC maturation.

In summary, our analysis defines changes in proliferative status of the developing HSC lineage at pre-liver stages beginning from E9.5. We found that dramatic expansion of maturing HSCs correlates with their active proliferation, likely driven by c-Kit/SCF signalling. Proliferative analysis revealed previously concealed heterogeneity within the pre-HSC populations. We describe the proliferative organisation of intra-aortic clusters that correlates with the functionally defined status of HSC

precursors. This study lays a foundation for molecular analysis of mechanisms underlying HSC development within intra-aortic clusters.

Experimental Procedures

Mice

Mice were housed and bred in animal facilities at the University of Edinburgh in compliance with UK Home Office Regulations. Embryos for experiments were obtained from intercrossing heterozygous hCdt1(30/120) -mKO2 (#610) and hGeminin(1/110)-mAG (#474) mice (Sakaue-Sawano et al. 2008; Yo et al. 2015b; Zielke & Edgar 2015) or from C57BL/6 CD45.2/2 mice. The day of discovery of the vaginal plug was designated as day 0.5. The embryos were additionally staged based on somite pair numbers (E9.5 = 26-29sp, E10.5 = 30-38 sp, E11.5 = 41-45 sp). C57BL/6 CD45.1/2 mice were used as transplant recipients and C57BL/6 CD45.1/1 as a source of carrier cells. All experiments with animals were approved under a Project License granted by the Home Office (UK), University of Edinburgh Ethical Review Committee, and conducted in accordance with local guidelines.

Flow cytometry and cell sorting

Single cell suspensions from the AGM region or foetal liver were prepared by dispase/collagenase-mediated dissociation, while single cell suspensions from bone marrow were obtained by flushing the tibias and femurs with a 26-gauge syringe needle (BD Microlance). Antibodies used for staining of cells were: anti-CD45-BV450 or BV650 (BD Horizon, clone 30F11), anti-VE-cadherin-A647 (Biolegend, Clone eBioBV13), biotinylated anti-VE-Cadherin (clone 11.D4.1) followed by incubation with streptavidin-APC (BD Pharmingen), anti-CD43-PE or anti-CD43-biotinylated (ebioscience, clone eBioR2/60) followed by incubation with streptavidin-BV650 (Biolegend), anti-CD41-PE or BV421 (Biolegend, clone MWReg30), anti-Sca1-BV421 or PE-Cy7 (eBioscience, clone D7), anti-c-Kit/CD117-BV421 (Biolegend, clone 2B8), anti-CD150-APC (Biolegend, clone TC15-12F12.2), anti-CD48-PerCPefluor710 (Biolegend, clone HM48-1), anti-Ki67-AF647 (BD Pharmingen, clone B56), 4-6 Diamidino-2-phenylindone (DAPI) (Biotium), anti-Ter119-PerCp-Cy5.5 or anti-Ter119-biotinylated (eBioscience), biotinylated anti-B220/CD45R (eBioscience, clone RA3-6B2), biotinylated anti-CD3e (eBioscience, clone 145-2C11), biotinylated anti-Gr1 (eBioscience, clone RB6-8C5). Lineage depletion

of bone marrow and foetal liver samples was performed by streptavidin particles (BD IMag) according to the manufacturer's instructions. 7-aminoactinomycin D viability staining solution, live-dead dye Zombie Aqua (Biolegend) or Infra-Red (Invitrogen) were used to exclude dead cells and gates were set using appropriate fluorescence minus one (FMO) controls. Flow cytometry analysis was performed on a Fortessa LSR using FACSDiva software, while analysis was done using FlowJo 10. Sorting was performed on a FACSAriaII using FACSDiva software. Correlation analysis between c-Kit levels and cell cycle phases was performed using GraphPad Prism. The different cell cycle fractions were plotted against c-Kit in FlowJo and segmented in equal parts across the c-Kit axis. The cell numbers with each segment/gate were extracted from FlowJo and used for the correlation analysis. A correlation coefficient (r) of +1 indicates perfect positive correlation (i.e. when X increases, then Y increases), whereas -1 shows negative/inverse correlation (i.e. when X increases, then Y decreases). A correlation coefficient of 0 shows that the two variables do not vary together at all. R squared or coefficient of determination is the fraction of the variance in the two variables that is shared. The p values in this analysis show whether the correlation is due to random sampling. Nonlinear regression analysis was used to draw a graph with a smooth curve that fits the data.

OP9 co-aggregates

E9.5 caudal parts or E10.5-11.5 AGM regions were isolated and for some experiments they were sub-dissected into AoV, AoD and UGRs. The notochord was included in the AoD. Sorted populations were co-aggregated with OP9 stromal cells as previously described (Rybtsov et al. 2011; Rybtsov et al. 2014). In all experiments, 1ee of sorted cells was co-aggregated with 100,000 OP9 cells. Cell aggregates were cultured at the liquid-gas interface on 0.8µm mixed cellulose MF-membranes (AAWP02500, Millipore) for 5-7 days (37ºC, 5% CO2) in 5ml of Iscove Modified Dulbecco Medium (IMDM, Invitrogen), 20% foetal calf serum (HyClone, ThermoScientific) supplemented with L-glutamine (4mM), penicillin/streptomycin (50 units/ml) and 100ng/ml SCF, 100ng/ml IL3, 100ng/ml Flt3l (all purchased from Peprotech). Suitable batches of foetal calf serum supporting effective maturation of pre-HSCs were selected after pre-testing in preliminary transplantation experiments (Taoudi et al. 2008) . Cells

from E9.5-10.5 AGM regions were cultured for 7 days, while cells from E11.5 AGM regions were cultured for 5 days.

HSC transplantation and CFU-C assay

AGM tissues from C57BL/6 CD45.2/2 embryos were pooled and cell suspensions obtained after dissociation with collagenase/dispase (Roche) for 40min at 37ºC. Dissociated cells were plated in methylcellulose culture which contains cytokines (MethoCult3434 medium; STEMCELL Technologies) according to the manufacturer's instructions. Donor cells were injected intravenously into C57BL/6 CD45.1/2 sub-lethally irradiated (1150 rad) mice along with 20000 C57BL/6 CD45.1/1 bone marrow carrier cells. The amount of transplanted cells is expressed in embryo equivalents (ee), defined as a unit of cells equivalent to the number present in one organ (e.g. 0.2ee corresponds to 20% of cells present in one AGM region). The number of ee injected for each experiment was chosen based on the expected outcome of dHSC numbers, which can vary for a given tissue depending on the developmental stage.

Long-term haematopoietic repopulation by donor cells was assessed in peripheral blood between 14 and 16 weeks after transplantation. Peripheral blood was collected by bleeding the tail vein into 500µl of 5mM EDTA/PBS. Erythrocytes were depleted using PharM Lyse (BD). Cells were stained with anti-CD16/32 (Fc-block), anti-CD45.1-V450 (cloneA20) and anti-CD45.2-APC (clone 104) monoclonal antibodies (eBioscience) and analyzed using a FACSCalibur. Data were analyzed in FlowJo software (TreeStar). Mice exhibiting >5% of donor chimerism were considered to be repopulated with dHSCs. Different groups of repopulated mice were compared using one-way ANOVA or t-test (*: $p<0.05$; **: $p<0.01$; ***: $p<0.005$; ****: $p<0.0001$).

Immunofluorescence

Whole-mount immunostaining was performed as previously described (Yokomizo et al., 2012) with slight modifications. Embryos dissected from the yolk sac and amnion were fixed with 2% PFA or cold acetone and, following dehydration by increasing concentrations of methanol, the head, limbs, and one

body wall were removed. After rehydration in 50% methanol, washing with PBS and blocking in 50% foetal calf serum/0.5% Triton X-100, the samples were incubated overnight with antibodies. For staining with antibodies from the same species, incubations were performed sequentially. Primary antibodies used were unconjugated goat anti-mouse CD43 (Santa Cruz, clone M19), rat anti-mouse VE-cadherin (BD Pharmingen, clone 11D4.1), rat anti-mouse CD45 (BD Pharmingen, clone 30-F11), rabbit anti-mouse RUNX1 (Abcam, clone EPR3099), rat anti-mouse CD41 (BD Pharmingen, clone MWReg30), rat anti-mouse c-Kit (Biolegend, clone 2B8), rabbit anti-mouse Ki67 (Abcam, clone SP6), rat anti-mouse phosphor-histone3 (Sigma, clone HTA28), rabbit anti-mAG (MBL International), rabbit anti-mKO2 (MBL International) and these were detected by the secondary antibodies anti-goat NL557 (R&D), anti-rat Alexa Fluor 647 (Invitrogen), or anti-rat Alexa 488 (Invitrogen) and anti-rabbit Alexa Fluor 647 (Abcam). After washing, the embryos were dehydrated with methanol and cleared with BABB (one part benzyl alcohol, two parts benzyl benzoate) solution (Yokomizo & Dzierzak, 2010). Secondary antibody only controls were used in all the experiments. Imaging of live sections was performed as previously described (Boisset et al. 2011) with slight modifications. Mouse embryos E10.5 were dissected and cut into slices of 300μm thickness using a tissue chopper. Slices were stained against c-Kit-APC (eBioscience, clone 2B8) for 10min at 4°C, then placed in Glass Bottom Dishes (MatTek) and covered with low melting point agarose gel (4%). The gel was then covered with IMDM without Phenol Red. Images were acquired with an inverted confocal microscope (Leica SP8) and processed using Volocity software.

Figure legends

Figure 1. **Changes in proliferative status of developing HSCs**.

(A) Representation of cell cycle analysis by Fucci reporters. (B) Experimental design of transplantation assays of pro-/pre-HSCs and dHSCs. (C) Flow cytometry analysis of HSC precursors and committed progenitors in Fucci embryos at different developmental stages (3 independent experiments) shown by bar graphs and representative dot plots. All the populations analysed are gated on Live Ter119^{-} cells. The pro-HSC population is identified as VC^{+}CD45^{-}CD41^{lo}CD43^{-}, while the progenitors are VC^{+}CD45^{-}

$CD41^{lo}CD43^{+}$. The pre-HSC Type I population is identified as $VC^{+}CD45^{-}CD41^{lo}CD43^{+}$, while the E10.5 progenitors are $VC^{+}CD45^{+}$. The pre-HSC Type II population is identified as $VC^{+}CD45^{+}CD41^{lo}CD43^{+}$ and the E11.5 progenitors as $VC^{-}CD45^{+}$. (D) Transplantation assays of pro-/pre-HSCs and dHSCs after sorting on the basis of the Geminin-mAG reporter (3 independent experiments). (E) Transplantation assays of foetal liver (LSK $CD48^{-}$) HSCs and bone marrow (LSK $CD150^{+}CD48^{-}$) HSCs after sorting on the basis of the Fucci reporters (3 independent experiments). The dashed line shows the 5% threshold. *p=0.02, **p=0.005, ***p=0.0006, ****p<0.0001. See also Fig. S1 & Table S1.

Figure 2. **Localisation and cell cycle status of $CD41^{+}Runx1^{+}$ cells in the E9.5 embryo.**

(A), (A′) Wild type E9.5 embryos stained against Runx1 and CD41. Low magnification (A) image shows the dorsal aorta and OMA, while high magnification (A′) shows the localisation of $VC^{+}CD41^{+}Runx1^{+}$ single cells in the dorsal aorta. (B) Geminin-mAG and (B′) Cdt1-mKO2 embryos stained against CD41 showing that pro-HSC phenotype cells (white arrows) in the dorsal aorta are in G_0/G_1. (C) Geminin-mAG and (C′) Cdt1-mKO2 embryos stained against CD43 showing that progenitors ($VC^{+}CD43^{+}$) are specifically localised in OMA and they are Geminin-mAG^{+}Cdt1-$mKO2^{-}$. Ao, dorsal aorta. Scale bar, 10 μm. See also Fig. S2.

Figure 3. Proliferative structure of intra-aortic haematopoietic clusters.

(A) E10.5 live section of Fucci embryo showing that cells at the base of the cluster are Geminin-mAG^{+}Cdt1-$mKO2^{-}$ (white arrowheads). (B, C) Geminin-mAG and (B′, C′) Cdt1-mKO2 embryos stained for CD43 (B, B′) at E10.5 and CD45 (C, C′) at E11.5 to identify pro-/pre-HSCs. (D) Wild type embryos stained against Ki67. White arrowheads show the cells at the base of the cluster. Scale bar, 10 μm. See also Fig. S2, S3 & S4.

Table 1. Proliferative structure of intra-aortic haematopoietic clusters.

Intra-aortic clusters counted in (A) E10.5 and (B) E11.5 Cdt1-mKO2 embryos stained against CD45 and VC. The total number of clusters as well as the number/percentage of clusters with slowly cycling $VC^{+}CD45^{-}Cdt1^{+}$ base counted is shown in the table.

Figure 4. c-Kit expression correlates with cell cycle status in HSC precursors.

Localisation and intensity of c-Kit expression in intra-aortic haematopoietic clusters in E10.5 (A) Geminin-mAG and (A′) Cdt1-mKO2 embryos. White arrowheads show c-Kit^{hi} and Geminin-mAG^{+} (or in A′, Cdt1-mKO2^{-}), while white arrows show c-Kit^{lo} and Cdt1-mKO2^{+} (or in A, Geminin-mAG^{-}). (B) Representative dot plots of flow cytometry analysis of E11.5 AGM pre-HSCs and correlation of c-Kit expression level with cell cycle status. Scale bar, 10μm. See also Fig. S3 & S4.

Figure 5. Changes and heterogeneity in proliferative status of the developing HSC lineage and their organisation within the intra-aortic clusters.

(A) Analysis of Fucci reporter mice defined changes in the proliferative status of the HSC precursors during development. The dramatic expansion of the pre-HSC pool during E10.5 correlates with their active proliferation. There might be two scenarios in order to explain the appearance of slowly cycling pre-HSC Type I in E11.5 AGM region; scenario A) a fraction of proliferative E10.5 pre-HSCs Type I slows down their cycling and persists as Type I until E11.5 and scenario B) this is a retarded E9.5 pro-HSC fraction which matured into pre-HSC Type I while maintaining their slow cycling. Also dHSCs are slowly cycling like their foetal liver counterparts, while the adult bone marrow HSCs are quiescent. (B) Slowly cycling cells are frequently found at the base of intra-aortic clusters, while more rapidly cycling cells are located at more apical positions. The proliferative organisation of intra-aortic clusters correlates with functionally defined status of HSCs and is suggested that these clusters grow through predominant expansion of more mature pre-HSCs. FL, foetal liver; BM, bone marrow; P, pro-HSC; I, pre-HSC Type I; II, pre-HSC Type II; H, dHSC.

Authorship

Contribution: AB, SR, CS, ABC, DH and SZ performed experiments. AB analysed data and made figures. PT provided important advice and support. AB and AM designed the research. AB and AM wrote the paper.

Conflict-of-interest disclosure: The authors declare no competing financial interests.

Correspondence: Alexander Medvinsky, Institute for Stem Cell Research, Medical Research Council

Centre for Regenerative Medicine, University of Edinburgh, SCRM Bioquarter, 5 Little France Drive, Edinburgh EH16 4UU, Scotland, UK. Email: A.Medvinsky@ed.ac.uk.

Acknowledgements

The authors thank J. Verth, C. Manson, J. Agnew and R. McInnis for assistance with mouse maintenance and breeding; C. Watt., C. Flockhart, C. Forrest, A. Dyer for irradiations; O. Rodriguez, Fiona Rossi and Claire Cryer for cell sorting; V. Berno and B. Vernay for help with microscopy. We thank A. Sakaue-Sawano for providing Fucci reporter mice. We thank Sergey Zuyev for helpful discussions on the correlation analysis. We thank S. Gordon-Keylock, A. McGarvey, J. Easterbrook and S. Heinrichs for helpful comments. This work was supported by Bloodwise (former LLR), BBSRC, MRC, Wellcome Trust.

References

Bashamboo, A. et al., 2006. The survival of differentiating embryonic stem cells is dependent on the SCF-KIT pathway. *Journal of cell science*, 119(Pt 15), pp.3039–3046.

Benz, C. et al., 2012. Hematopoietic stem cell subtypes expand differentially during development and display distinct lymphopoietic programs. *Cell Stem Cell*, 10(3), pp.273–283.

Boisset, J. et al., 2015. Progressive maturation toward hematopoietic stem cells in the mouse embryo aorta. , 125(3), pp.465–470.

Boisset, J.-C. et al., 2011. Ex vivo time-lapse confocal imaging of the mouse embryo aorta. *Nature protocols*, 6(11), pp.1792–805.

Bowie, M.B. et al., 2006. Hematopoietic stem cells proliferate until after birth and show a reversible phase-specific engraftment defect. *Journal of Clinical Investigation*, 116(10), pp.2808–2816.

Bowie, M.B. et al., 2007. Identification of a new intrinsically timed developmental checkpoint that reprograms key hematopoietic stem cell properties. *Proceedings of the National Academy of Sciences of the United States of America*, 104(14), pp.5878–5882.

Bowie, M.B. et al., 2007. Steel factor responsiveness regulates the high self-renewal phenotype of fetal hematopoietic stem cells. *Blood*, 109(11), pp.5043–5048.

Budirahardja, Y. & Gönczy, P., 2009. Coupling the cell cycle to development. *Development (Cambridge, England)*, 136(17), pp.2861–2872.

Ciau-Uitz, A., Patient, R. & Medvinsky, A., 2016. Ontogeny of the Hematopoietic System. In *Encyclopedia of Immunobiology*. pp. 1–14.

Ding, L. et al., 2012. Endothelial and perivascular cells maintain haematopoietic stem cells. *Nature*, 481(7382), pp.457–62.

Dykstra, B. et al., 2007. Long-Term Propagation of Distinct Hematopoietic Differentiation Programs In Vivo. *Cell Stem Cell*, 1(2), pp.218–229.

Ema, H. et al., 2000. In vitro self-renewal division of hematopoietic stem cells. *The Journal of experimental medicine*, 192(9), pp.1281–1288.

Ema, H., Morita, Y. & Suda, T., 2014. Heterogeneity and hierarchy of hematopoietic stem cells. *Experimental Hematology*, 42(2), pp.74–82.

Ema, H. & Nakauchi, H., 2000. Expansion of hematopoietic stem cells in the developing liver of a mouse embryo. *Blood*, 95(7), pp.2284–8.

Fuchs, E., 2009. The Tortoise and the Hair: Slow-Cycling Cells in the Stem Cell Race. *Cell*, 137(5), pp.811–819.

Garcia-Porrero, J., Godin, I. & Dieterlen-Lièvre, F., 1995. Potential intraembryonic hemogenic sites at pre-liver stages in the mouse. *Anat Embryol (Berl)*, 192(5), pp.423–35.

Gordon-Keylock, S. et al., 2013. Mouse extraembryonic arterial vessels harbor precursors

capable of maturing into definitive HSCs. *Blood*, 122(14), pp.2338–2345.

Ikuta, K. & Weissman, I.L., 1992. Evidence that hematopoietic stem cells express mouse c-kit but do not depend on steel factor for their generation. *Proceedings of the National Academy of Sciences of the United States of America*, 89(4), pp.1502–1506.

Jude, C.D. et al., 2008. Leukemia and hematopoietic stem cells: Balancing proliferation and quiescence. *Cell Cycle*, 7(5), pp.586–591.

Kaldis, P. & Richardson, H.E., 2012. When cell cycle meets development. *Development*, 139(2), pp.225–230.

Kiel, M.J. et al., 2005. SLAM family receptors distinguish hematopoietic stem and progenitor cells and reveal endothelial niches for stem cells. *Cell*, 121(7), pp.1109–1121.

Kissa, K. & Herbomel, P., 2010. Blood stem cells emerge from aortic endothelium by a novel type of cell transition. *Nature*, 464(7285), pp.112–115.

Kumaravelu, P. et al., 2002. Quantitative developmental anatomy of definitive haematopoietic stem cells/long-term repopulating units (HSC/RUs): role of the aorta-gonad-mesonephros (AGM) region and the yolk sac in colonisation of the mouse embryonic liver. *Development (Cambridge, England)*, 129(21), pp.4891–4899.

Lange, C. & Calegari, F., 2010. Cdks and cyclins link G1 length and differentiation of embryonic, neural and hematopoietic stem cells. *Cell Cycle*, 9(10), pp.1893–1900.

Lange, C., Huttner, W.B. & Calegari, F., 2009. Cdk4/cyclinD1 overexpression in neural stem cells shortens G1, delays neurogenesis, and promotes the generation and expansion of basal progenitors. *Cell stem cell*, 5(3), pp.320–31.

Liakhovitskaia, a. et al., 2014. Runx1 is required for progression of CD41+ embryonic precursors into HSCs but not prior to this. *Development*, 141(17), pp.3319–3323.

Marcelo, K.L. et al., 2013. Hemogenic endothelial cell specification requires c-Kit, Notch

signaling, and p27-mediated cell-cycle control. *Developmental cell*, 27(5), pp.504–15.

Matsuoka, Y. et al., 2011. Low level of C-kit expression marks deeply quiescent murine hematopoietic stem cells. *Stem Cells*, 29(11), pp.1783–1791.

Medvinsky, A. & Dzierzak, E., 1996. Definitive hematopoiesis is autonomously initiated by the AGM region. *Cell*, 86(6), pp.897–906.

Medvinsky, A., Rybtsov, S. & Taoudi, S., 2011. Embryonic origin of the adult hematopoietic system: advances and questions. *Development (Cambridge, England)*, 138(6), pp.1017–1031.

Mendelson, A. & Frenette, P.S., 2014. Hematopoietic stem cell niche maintenance during homeostasis and regeneration. *Nature medicine*, 20(8), pp.833–46.

Morrison, S.J. & Scadden, D.T., 2014. The bone marrow niche for haematopoietic stem cells. *Nature*, 505(7483), pp.327–34.

Müller, A.M. et al., 1994. Development of hematopoietic stem cell activity in the mouse embryo. *Immunity*, 1(4), pp.291–301.

Nakamura-Ishizu, a., Takizawa, H. & Suda, T., 2014. The analysis, roles and regulation of quiescence in hematopoietic stem cells. *Development*, 141(24), pp.4656–4666.

North, T. et al., 1999. Cbfa2 is required for the formation of intra-aortic hematopoietic clusters. *Development (Cambridge, England)*, 126(11), pp.2563–2575.

Nygren, J.M., Bryder, D. & Jacobsen, S.E.W., 2006. Prolonged Cell Cycle Transit is a Defining and Developmentally Conserved Hemopoietic Stem Cell Property. *The Journal of Immunology*, 177, pp.201–208.

Parish, C.R., 1999. Fluorescent dyes for lymphocyte migration and proliferation studies. *Immunology and cell biology*, 77(6), pp.499–508.

Passegué, E. et al., 2005. Global analysis of proliferation and cell cycle gene expression in

the regulation of hematopoietic stem and progenitor cell fates. *The Journal of experimental medicine*, 202(11), pp.1599–1611.

Pauklin, S. & Vallier, L., 2013. The Cell-Cycle State of Stem Cells Determines Cell Fate Propensity. *Cell*, 155(1), pp.135–147.

Pietras, E.M., Warr, M.R. & Passegue, E., 2011. Cell cycle regulation in hematopoietic stem cells. *The Journal of Cell Biology*, 195(5), pp.709–720.

Rybtsov, S. et al., 2016a. Concealed expansion of immature precursors underpins acute burst of adult HSC activity in foetal liver. *Development (Cambridge, England)*, 143(8), pp.1284–9.

Rybtsov, S. et al., 2016b. Concealed expansion of immature precursors underpins acute burst of adult HSC activity in foetal liver. *Development (Cambridge, England)*, 143(8), pp.1284–9.

Rybtsov, S. et al., 2011. Hierarchical organization and early hematopoietic specification of the developing HSC lineage in the AGM region. *The Journal of experimental medicine*, 208(6), pp.1305–1315.

Rybtsov, S. et al., 2014. Tracing the Origin of the HSC Hierarchy Reveals an SCF-Dependent, IL-3-Independent CD43− Embryonic Precursor. *Stem Cell Reports*, 3(3), pp.489–501.

Sakaue-Sawano, A. et al., 2008. Visualizing Spatiotemporal Dynamics of Multicellular Cell-Cycle Progression. *Cell*, 132(3), pp.487–498.

Sasaki, T. et al., 2010. Regulation of hematopoietic cell clusters in the placental niche through SCF/Kit signaling in embryonic mouse. *Development (Cambridge, England)*, 137(23), pp.3941–52.

Seita, Jun; Weissman, I.L., 2010. Hematopoietic Stem Cell: Self-renewal versus Differentiation. *Wiley Interdiscip Rev Syst Biol Med*, 2(6), pp.640–653.

Shin, J.Y. et al., 2014. High c-Kit expression identifies hematopoietic stem cells with impaired self-renewal and megakaryocytic bias. *The Journal of experimental medicine*, 211(2), pp.217–231.

Sieburg, H.B. et al., 2010. The hematopoietic stem compartment consists of a limited number of discrete stem cell subsets The hematopoietic stem compartment consists of a limited number of discrete stem cell subsets. , 107(6), pp.2311–2316.

Souilhol, C. et al., 2016. Inductive interactions mediated by interplay of asymmetric signalling underlie development of adult haematopoietic stem cells. *Nature communications*, 7, p.10784.

Swiers, G. et al., 2013. Early dynamic fate changes in haemogenic endothelium characterized at the single-cell level. *Nature communications*, 4, p.2924.

Takizawa, H. et al., 2011. Dynamic variation in cycling of hematopoietic stem cells in steady state and inflammation. *Journal of Experimental Medicine*, 208(2), pp.273–284.

Taoudi, S. et al., 2008. Extensive hematopoietic stem cell generation in the AGM region via maturation of VE-Cadherin +CD45 + pre-definitive HSCs. *Cell Stem Cell*, 3(1), pp.99–108.

Taoudi, S. & Medvinsky, A., 2007. Functional identification of the hematopoietic stem cell niche in the ventral domain of the embryonic dorsal aorta. *Proceedings of the National Academy of Sciences of the United States of America*, 104(22), pp.9399–9403.

Thorén, L. a et al., 2008. Kit regulates maintenance of quiescent hematopoietic stem cells. *Journal of immunology*, 180(4), pp.2045–2053.

Wilson, A. et al., 2008. Hematopoietic Stem Cells Reversibly Switch from Dormancy to Self-Renewal during Homeostasis and Repair. *Cell*, 135(6), pp.1118–1129.

Yo, M. et al., 2015. Fucci-guided purification of hematopoietic stem cells with high repopulating activity. *Biochemical and Biophysical Research Communications*, 457(1), pp.7–11.

Yoder, M.C. et al., 1997. Characterization of definitive lymphohematopoietic stem cells in the day 9 murine yolk sac. *Immunity*, 7(3), pp.335–344.

Yokomizo, T. et al., 2012. Whole-mount three-dimensional imaging of internally localized immunostained cells within mouse embryos. *Nat.Protoc.*, 7(1750–2799 (Electronic)), pp.421–431.

Yokomizo, T. & Dzierzak, E., 2010. Three-dimensional cartography of hematopoietic clusters in the vasculature of whole mouse embryos. *Development (Cambridge, England)*, 137(21), pp.3651–3661.

Zhou, F. et al., 2016. Tracing haematopoietic stem cell formation at single-cell resolution. *Nature*, 533(7604), pp.1–17.

Zielke, N. & Edgar, B.A., 2015. FUCCI sensors: powerful new tools for analysis of cell proliferation. *Wiley interdisciplinary reviews. Developmental biology*, 4(5), pp.469–87.

Zovein, A.C. et al., 2010. Vascular remodeling of the vitelline artery initiates extravascular emergence of hematopoietic clusters. *Blood*, 116(18), pp.3435–3444.

Figure

Figure 1.

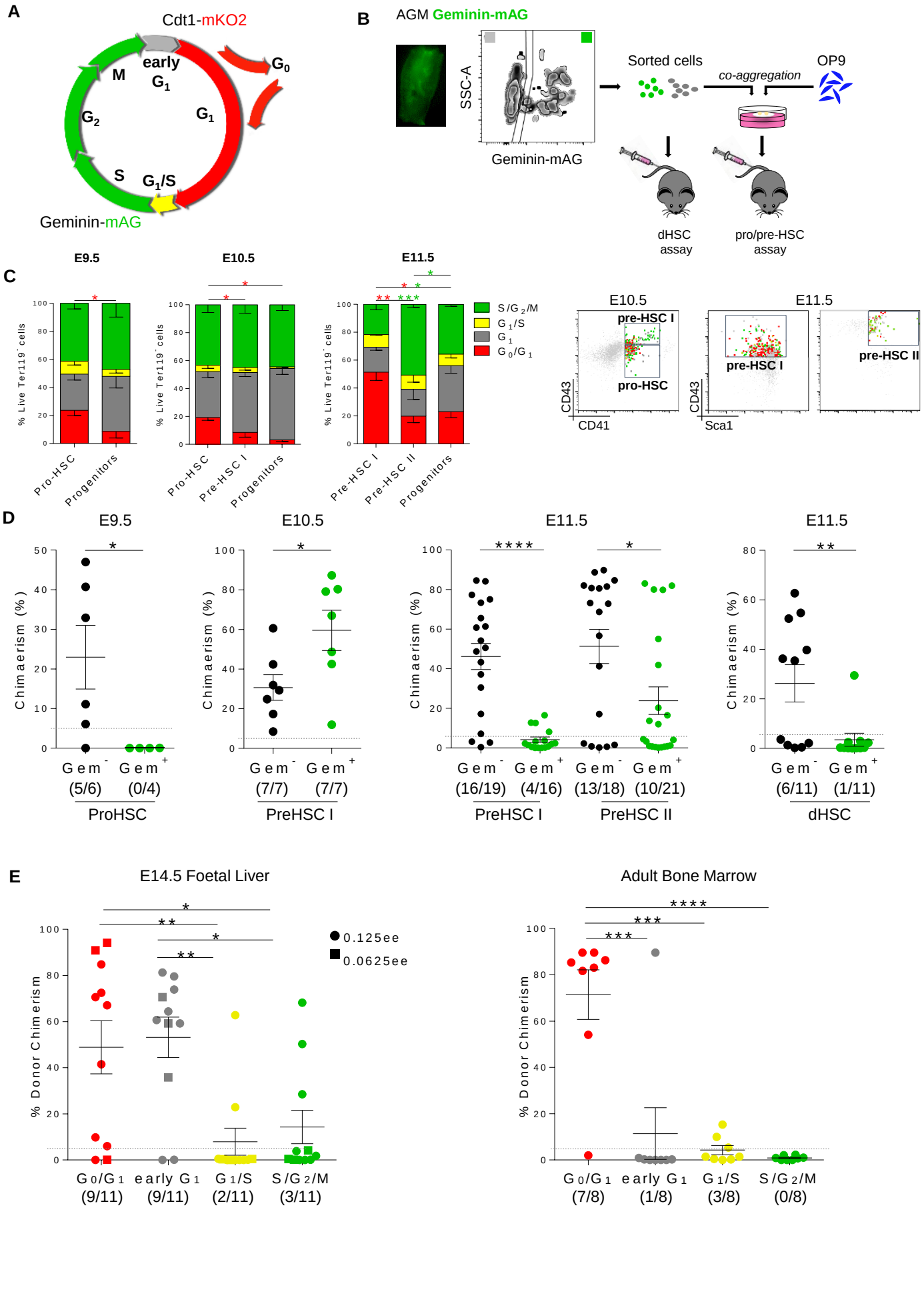

Figure 2.

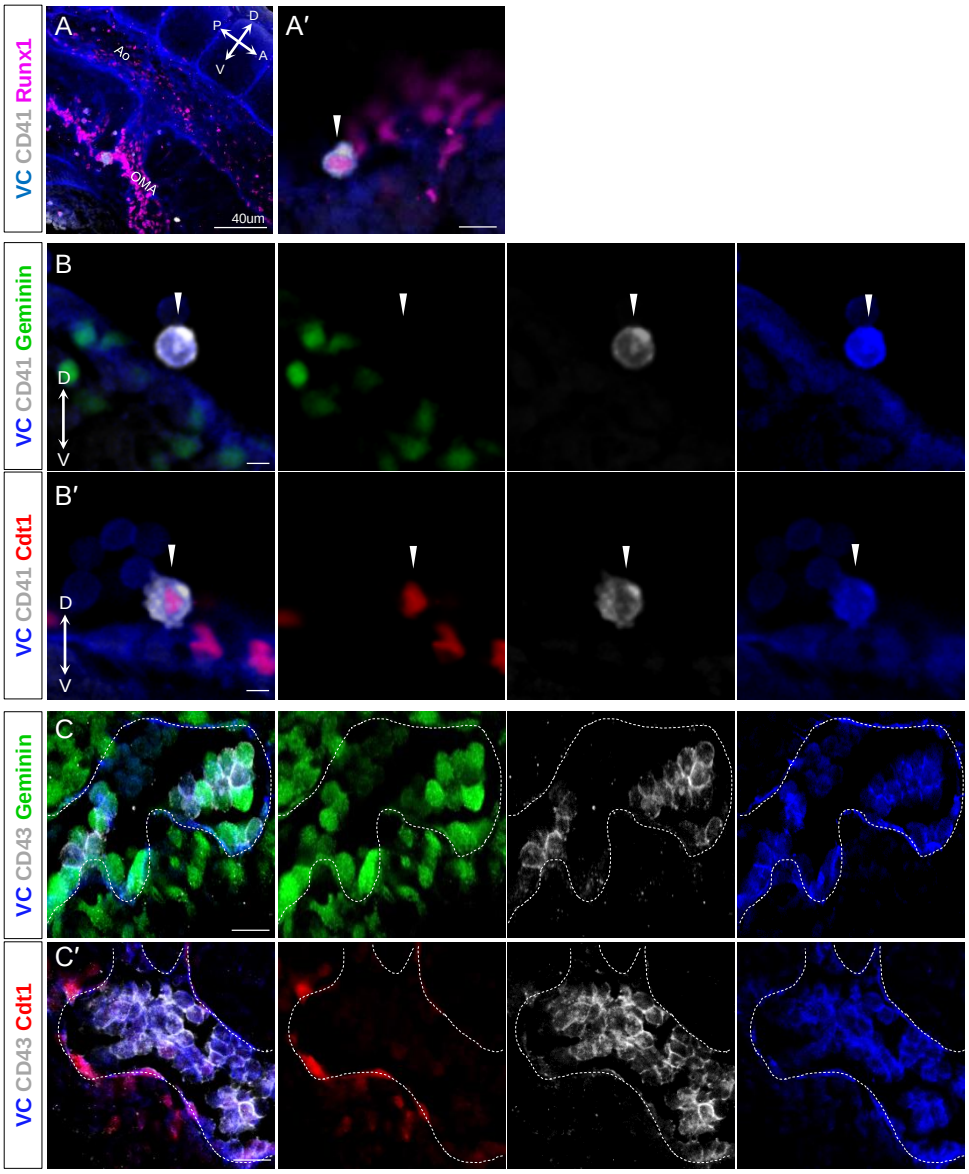
VC CD41 Runx1
A
Ao
P
D
V
A
DMA
40um
A′
VC CD41 Geminin
B
D
V
VC CD41 Cdt1
B′
D
V
VC CD43 Geminin
C
VC CD43 Cdt1
C′

Figure 3.

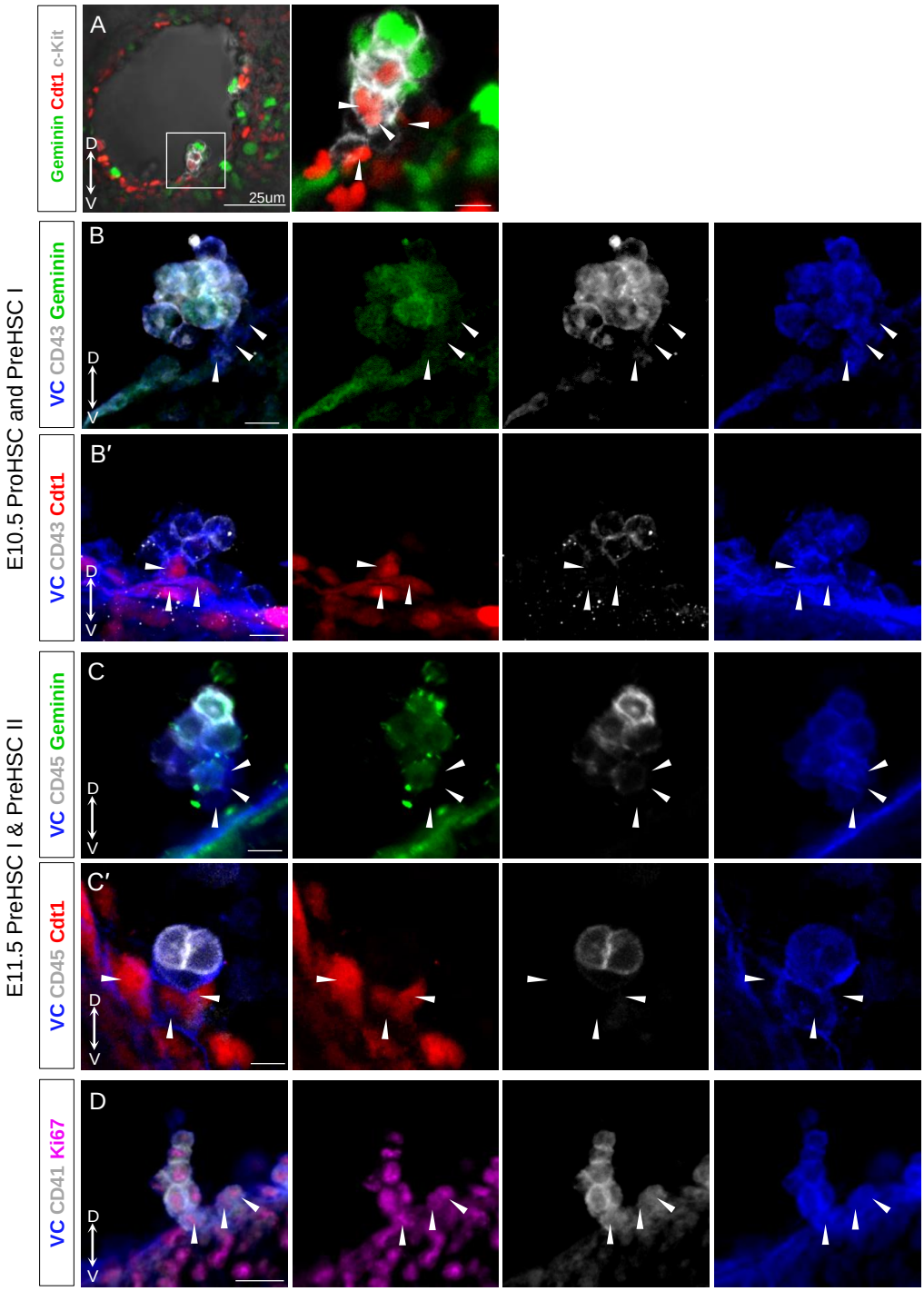
A
Geminin Cdt1 c-Kit
D
V
25um
B
VC CD43 Geminin
B′
VC CD43 Cdt1
E10.5 ProHSC and PreHSC I
C
VC CD45 Geminin
C′
VC CD45 Cdt1
E11.5 PreHSC I & PreHSC II
D
VC CD41 Ki67

Figure 4.

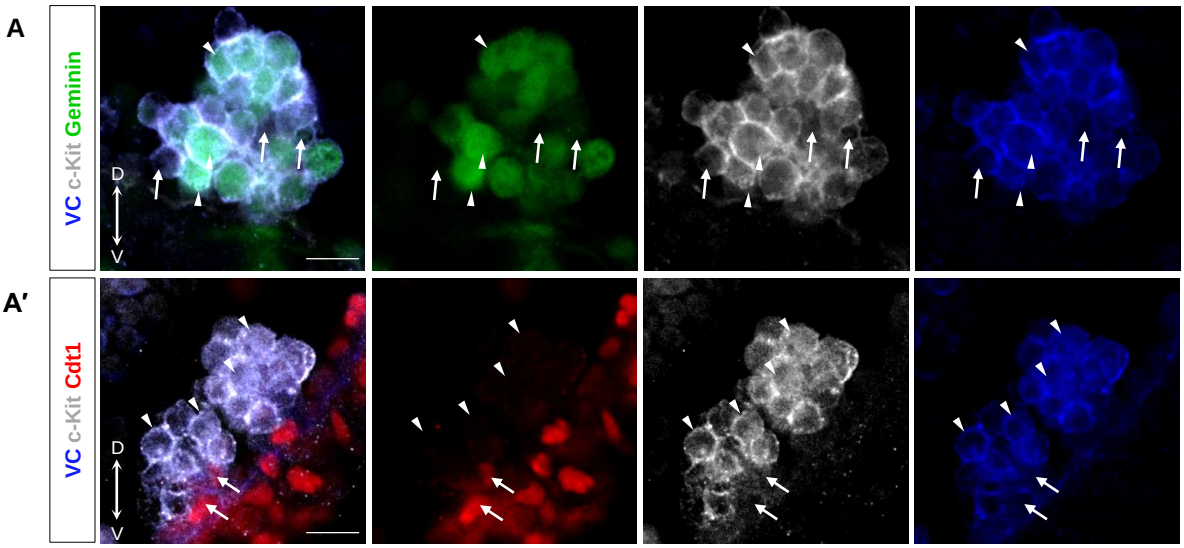
A
VC c-Kit Geminin
D
V
A'
VC c-Kit Cdt1
D
V

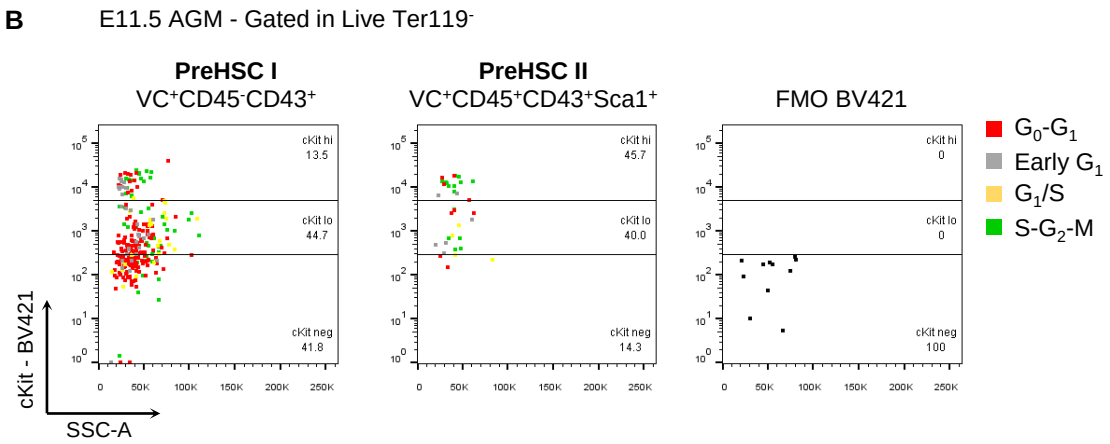
B
E11.5 AGM - Gated in Live Ter119-
PreHSC I
VC+CD45-CD43+
PreHSC II
VC+CD45+CD43+Sca1+
FMO BV421
cKit hi
13.5
cKit lo
44.7
cKit neg
41.8
cKit hi
45.7
cKit lo
40.0
cKit neg
14.3
cKit hi
0
cKit lo
0
cKit neg
100
cKit - BV421
SSC-A
G0-G1
Early G1
G1/S
S-G2-M

Figure 5.

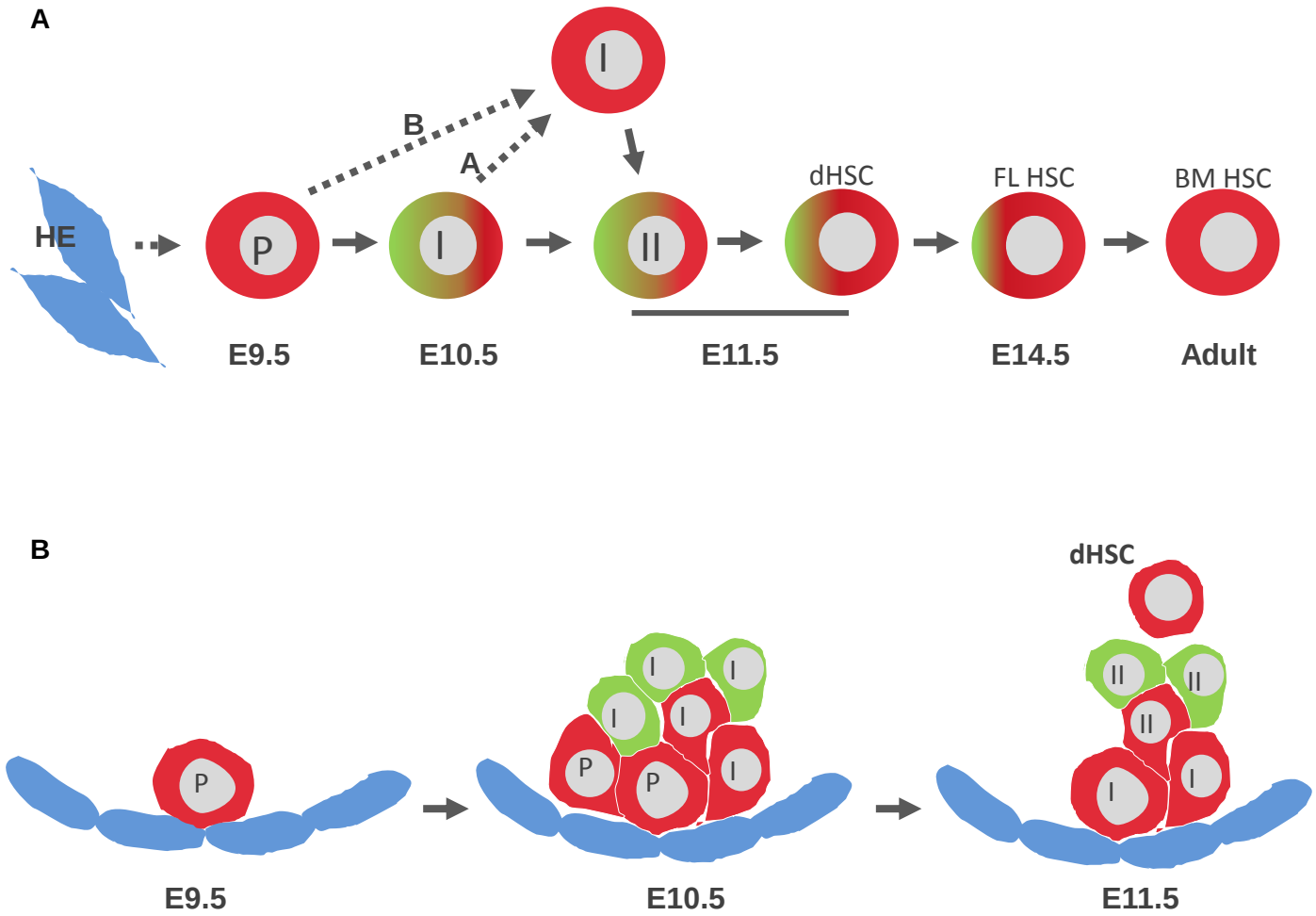
A
HE
P
I
II
B
A
dHSC
FL HSC
BM HSC
E9.5
E10.5
E11.5
E14.5
Adult
B
P
I
II
dHSC
E9.5
E10.5
E11.5

Table 1. Proliferative structure of intra-aortic haematopoietic clusters.

A

Sample E10.5	No. clusters with VC^+CD45^- $Cdt1^+$ base	Total No. clusters	% clusters with $Cdt1^+$ base
Embryo 1	12	12	100
Embryo 2	14	19	74
Embryo 3	21	24	87
Embryo 4	6	9	67

B

Sample E11.5	No. clusters with VC^+CD45^- $Cdt1^+$ base	Total No. clusters	% clusters with $Cdt1^+$ base
Embryo 1	4	5	80
Embryo 2	12	15	80
Embryo 3	6	15	40
Embryo 4	12	14	89
Embryo 5	3	5	60

Intra-aortic clusters counted in (A) E10.5 and (B) E11.5 Cdt1-mKO2 embryos stained against CD45 and VC. The total number of clusters as well as the number/percentage of clusters with slowly cycling $VC^+CD45^-Cdt1^+$ base counted is shown in the table.

Supplementary Figure 1. Related to Figure 1.

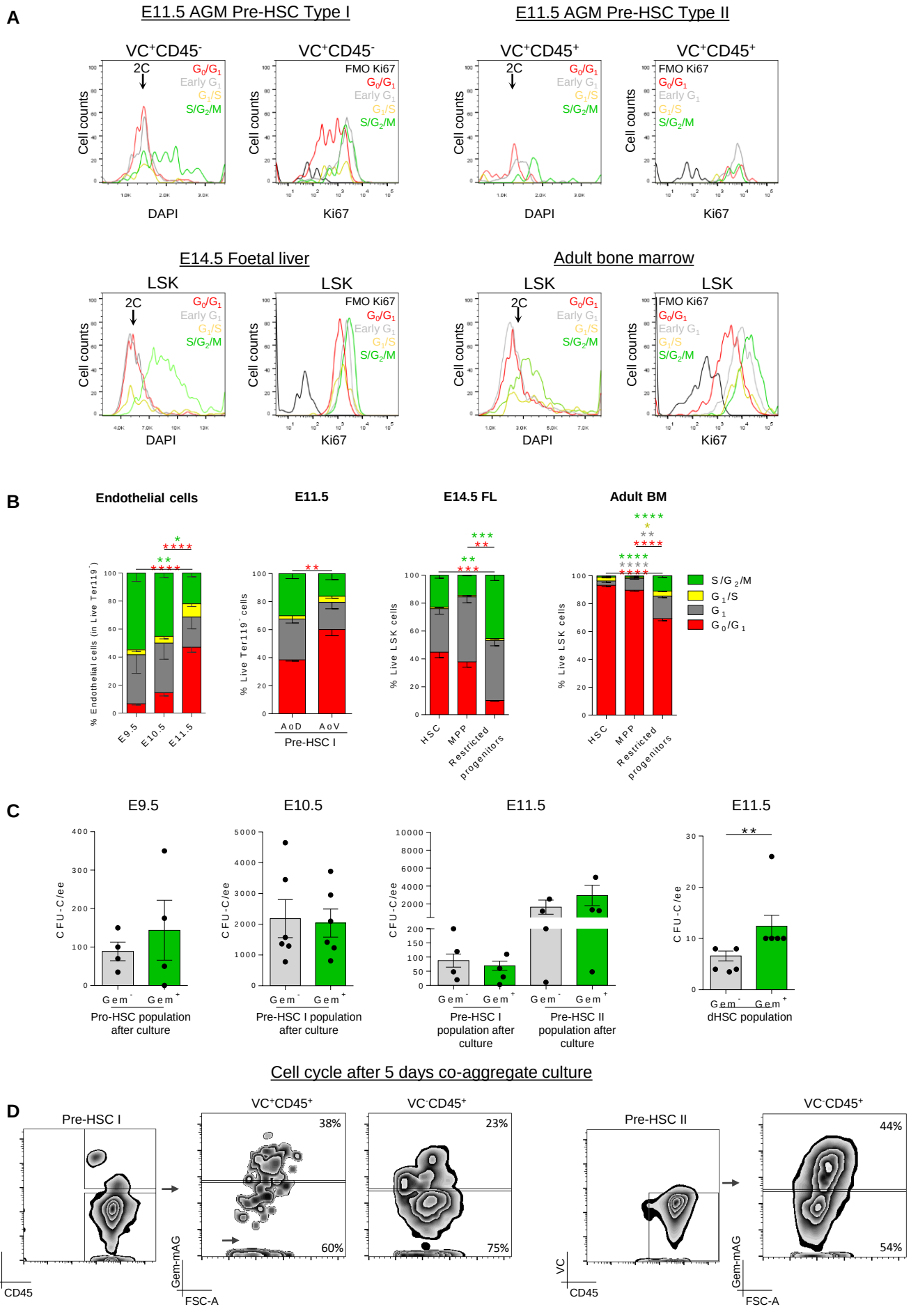

Supplementary Figure 1. Related to Fig. 1. **Validation of Fucci reporters and cell cycle analysis of haematopoietic populations.**

(A) Validation of the Fucci reporters (Geminin-mAG and Cdt1-mKO2) in haematopoietic populations at various stages with Ki67 and DAPI staining (2C, diploid DNA). All populations are gated on Live Lineage$^-$ cells. (B) Flow cytometry of various populations of Fucci embryos and adults. The endothelial population is identified as VC$^+$CD45$^-$CD41$^-$CD43$^-$ and the pre-HSC Type I population as VC$^+$CD45$^-$CD41$^-$CD43$^+$, in the AGM region. The HSC population is identified as LSK CD150$^+$CD48$^-$, the MPP as LSK CD150$^-$CD48$^-$ and the restricted progenitors as LSK CD150$^-$CD48$^+$, both in FL and BM. (C) In vitro methylcellulose assay of pro-/pre-HSC populations after co-aggregate culture and dHSC populations directly after sorting. (D) Representative flow cytometry plots of E11.5 pre-HSC I and II sorted populations after 5 days co-aggregate culture. Geminin-mAG$^{-/+}$ fractions had no difference in their output in terms of cell cycle. FL, foetal liver; BM, bone marrow. ** p=0.007, ***p=0.0006, ****p<0.0002.

Supplementary Figure 2. Related to figures 2 and 3

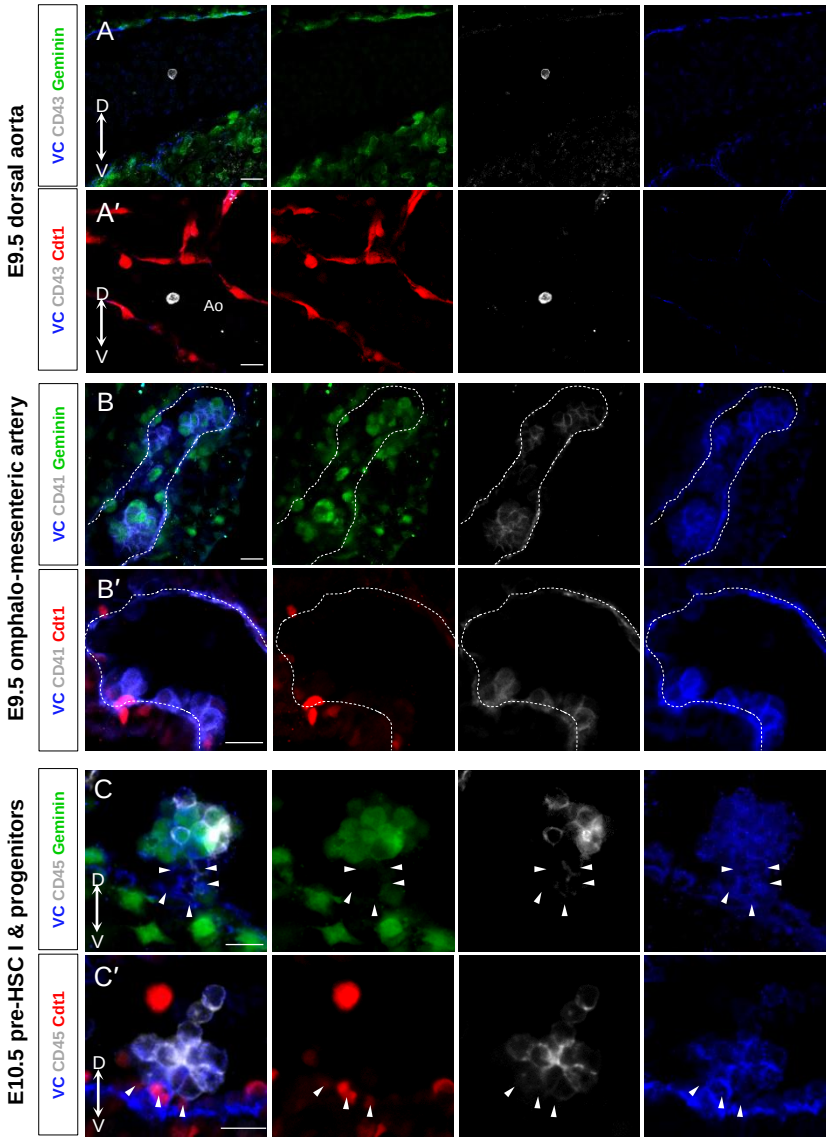

Supplementary Figure 2. Related to Fig. 2, 3. **E9.5 OMA and E10.5 intra-aortic clusters and their cell cycle status.**

(A), (B), (C) Geminin-mAG and (A′), (B′), (C′) Cdt1-mKO2 embryos stained for different haematopoietic markers. (A), (A′) CD43 is not expressed in the dorsal aorta of E9.5 embryos. (B), (B′) CD41 is expressed in the E9.5 OMA cell clusters, which are Geminin-mAG^{+}Cdt1-mKO2^{-}. (C), (C′) CD45 is localised at the top of the E10.5 intra-aortic clusters and marks mainly progenitors that are actively cycling (Geminin-mAG^{+}Cdt1-mKO2^{-}). Scale bar, 15 µm.

Supplementary Figure 3. Related to Figure 3.

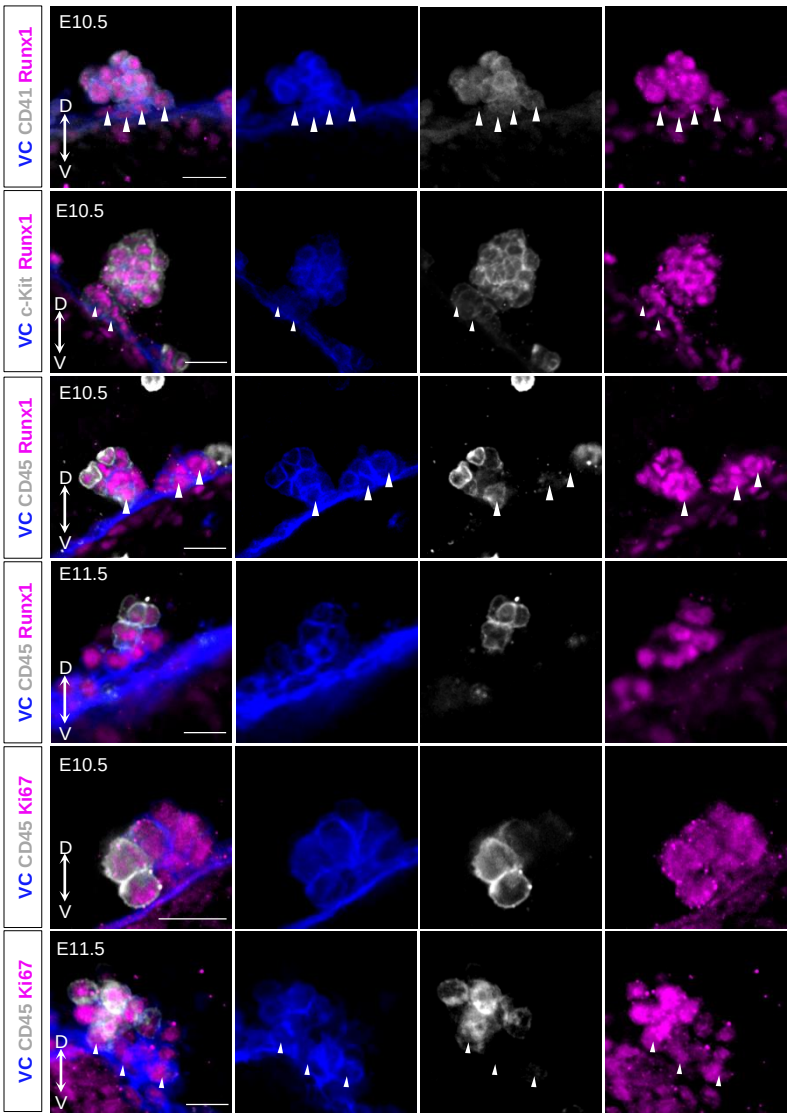

Supplementary Figure 3. Related to Fig. 3 & 4. **Characterisation of intra-aortic clusters with various haematopoietic markers.**

Representative images of wild type E10.5-11.5 embryos showing the expression pattern of Runx1, CD41, c-Kit, CD45 and Ki67 within intra-aortic clusters. Of note, the cells at the base of these clusters are haematopoietic (white arrowheads). Scale bar, 15 µm.

Supplementary Figure 4. Related to Figure 3 and 4.

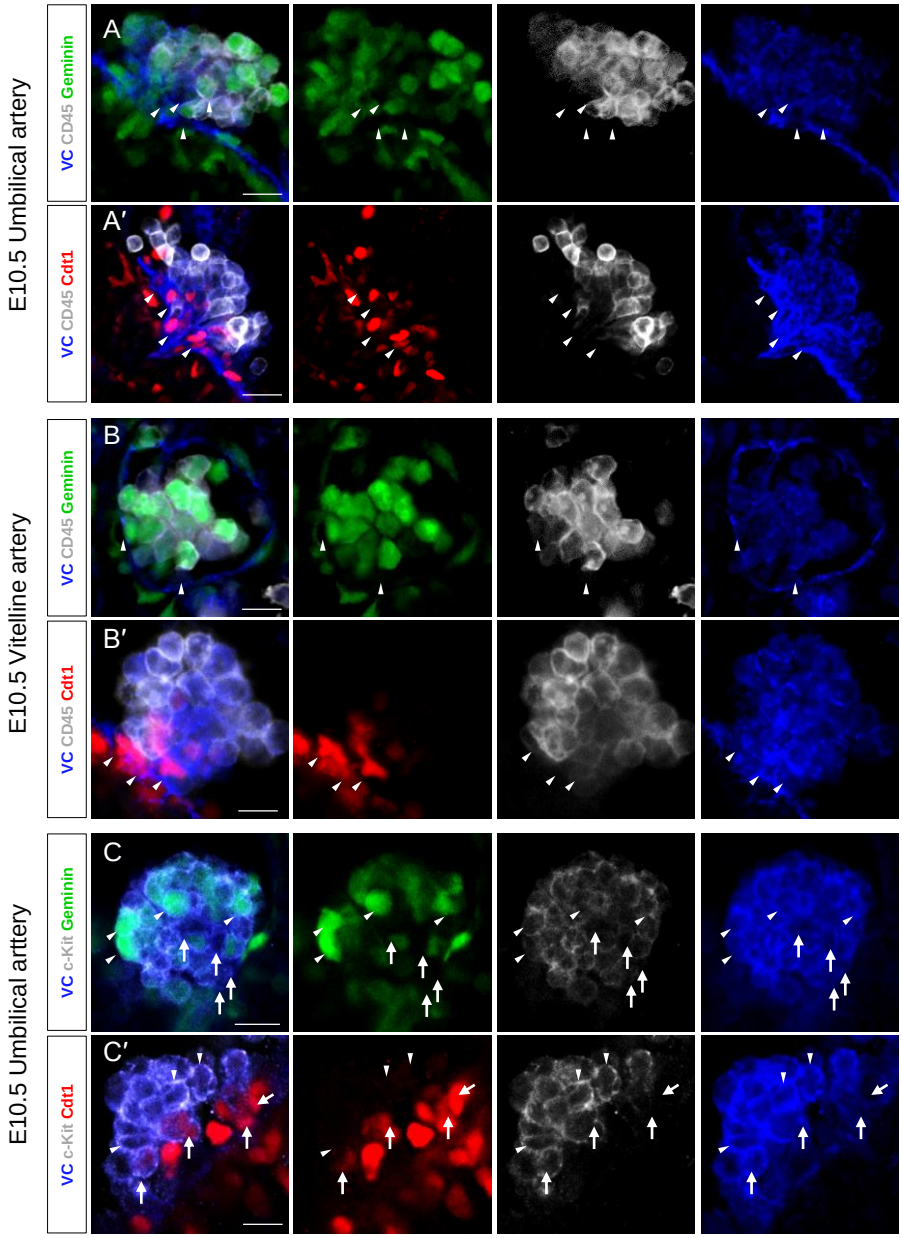

Supplementary Figure 4. Related to Fig. 3 & 4. **Cell cycle status of haematopoietic clusters in the extra-embryonic vessels.** (A), (B), (C) Geminin-mAG and (A′), (B′), (C′) Cdt1-mKO2 embryos stained for different haematopoietic markers. (A), (A′), (B), (B′) Representative images of haematopoietic clusters with slowly cycling cells (Geminin-mAG^{-}Cdt1-mKO2^{+}) at their base in umbilical and vitelline arteries (white arrowheads) in E10.5 embryos. (C), (C′) c-Kit expression in umbilical artery clusters showing that c-Kit^{lo} cells are Geminin-mAG^{-}Cdt1-mKO2^{+} (white arrows), while c-Kit^{hi} expressing cells are Geminin-mAG^{+}Cdt1-mKO2^{-} (white arrowheads). Scale bar, 10µm.

Supplementary Table 1. Related to Figure 1. Cell numbers for co-aggregate culture and transplantations.

A

Experiment	No. cells/ee (1 aggregate)		No. cells/aggregate after culture		Dose transplanted/ recipient
	Gem-mAG$^-$	Gem-mAG$^+$	Gem-mAG$^-$	Gem-mAG$^+$	
E9.5 pro-HSC Expt.1	130	36	66612	41244	4 ee
E9.5 pro-HSC Expt.2	32	20	65743	43956	5 ee
E10.5 pre-HSC I Expt.1	117	62	1231984	1060184	4 ee
E10.5 pre-HSC I Expt.2	131	56	934617	1226718	4 ee
E10.5 pre-HSC I Expt.3	181	91	1513570	892790	4 ee
E11.5 pre-HSC I Expt.1	1209	1041	43850	65710	1 ee
E11.5 pre-HSC I Expt.2	1475	960	39840	33010	1 ee
E11.5 pre-HSC I Expt.3	1381	314	29050	23710	1 ee
E11.5 pre-HSC I Expt.4	1346	935	48213	37854	1 ee
E11.5 pre-HSC I Expt.5	1399	521	26084	30588	1 ee
E11.5 pre-HSC II Expt.1	397	1041	69312	131835	1 ee
E11.5 pre-HSC II Expt.2	437	578	70966	87188	1 ee
E11.5 pre-HSC II Expt.3	794	332	94278	125761	1 ee
E11.5 pre-HSC II Expt.4	1143	771	80580	93525	1 ee
E11.5 pre-HSC II Expt.5	716	411	79890	89050	1 ee

B

Experiment	No. cells transplanted/recipient			
	Gem-mAG$^-$	Gem-mAG$^+$		
E11.5 dHSC Expt.1	20487	10471		
E11.5 dHSC Expt.2	45567	29463		
E11.5 dHSC Expt.3	32467	12610		
E11.5 dHSC Expt.4	102000	84500		
E11.5 dHSC Expt.5	182909	53090		
E11.5 dHSC Expt.6	137181	39181		
	G_0/G_1	Early G_1	G_1/S	$S/G_2/M$
E14.5 FL Expt.1	342	465	222	414
E14.5 FL Expt.2	455	426	356	453
E14.5 FL Expt.3	34	36	5	46
Adult BM Expt.1	6417	1839	183	1204
Adult BM Expt.2	1287	116	61	46

Supplementary Table 1. Related to Figure 1. **Cell numbers for co-aggregate culture and transplantations.**

(A) E9.5, 10.5 and 11.5 Geminin-mAG reporter embryos were sorted for pro-/pre-HSCs. Representative numbers of sorted cells used for one co-aggregate (1 ee), representative total cell numbers of one co-aggregate after culture and the dose transplanted in each experiment are shown in the table. (B) The number of sorted cells from E11.5 AGM region (Geminin-mAG reporter embryos), foetal liver and adult bone marrow (Fucci embryos and adults) that were transplanted directly in recipients is shown in this table.

Supplementary Table 2. Related to Figure 4. Correlation analysis of c-Kit low and high levels with different cell cycle fractions within the pre-HSC I population.

Correlation Analysis c-Kit low-high vs cell fractions					
	cKit vs G_0-G_1 (red)	**cKit vs early G_1** (grey)	**cKit vs G_1/S** (yellow)	**cKit vs S/G_2/M** (green)	**cKit vs ratio red/green**
r	-0.8	-0.5	-0.4	-0.1	-0.7
R square	0.7	0.3	0.1	0.02	0.5
P value (two-tailed)	0.0004	0.04	0.2	0.7	0.004
P value summary	***	*	ns	ns	**

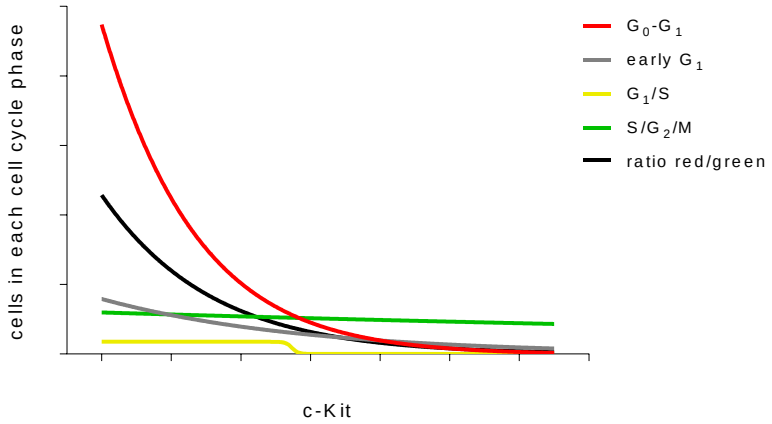

Supplementary Table 2. Related to Figure 4. **Correlation analysis of c-Kit low and high levels with different cell cycle fractions within the pre-HSC I population.**

(A) E11.5 Pre-HSC Type I population from double transgenic Fucci embryos was analysed for cell cycle status and c-Kit levels by flow cytometry. Cell numbers extracted from the FlowJo analysis were used for the correlation analysis performed with GraphPad. The table shows the correlation coefficient (r), the r square and the p value (see Experimental Procedures). Pre-HSC Type I cells in G_0/G_1 inversely correlate with c-Kit levels similar to cells in early G_1 phase. Also the ratio of (G_0/G_1 cells) / ($S/G_2/M$ cells) negatively correlate with c-Kit levels; therefore when c-Kit levels increase, the probability of G_0/G_1 cells within this fraction diminishes. On the contrary, there is no correlation between cells found in G_1/S and $S/G_2/M$ phases and c-Kit levels and thus change in one variable (i.e. cell cycle phase) does not cause change in the other variable (i.e. c-Kit levels). (B) Nonlinear regression lines fit these data and depict the negative correlation between slowly cycling (G_0/G_1 and early G_0) cells and c-Kit levels.